Contents lists available at ScienceDirect

Geochimica et Cosmochimica Acta

Schreibersite oxidation under varied oxygen buffers

Tian Feng [a], Arthur Omran [a,b], Maheen Gull [a], Micah J. Schaible [c], Thomas M. Orlando [c,d], Matthew A. Pasek [a,*]

[a] School of Geosciences, University of South Florida, NES 204, 4202 East Fowler Ave., Tampa, FL 33620, USA
[b] Department of Chemistry, University of North Florida, Jacksonville, FL 32224, USA
[c] School of Chemistry and Biochemistry, Georgia Institute of Technology, Atlanta, GA 30332, USA
[d] School of Physics, Georgia Institute of Technology, Atlanta, GA 30332, USA

ARTICLE INFO

ABSTRACT

Phosphorus is often present in meteorites as the mineral schreibersite, in which P is in a reduced oxidation state as a phosphide. Phosphides such as schreibersite have been proposed to be important to the development of life on the earth and may serve as indicators of metamorphic grade on meteorite parent bodies. Here we investigate how synthetic schreibersite (as the iron end-member, Fe_3P) oxidizes into calcium phosphates through reaction with silicates under high temperature conditions, at specific oxygen fugacities, and in the absence of water. We find that schreibersite readily oxidizes to phosphates at temperatures of 750–850 °C over a few weeks depending on the oxygen fugacity of the environment. The rate of this process is best matched by diffusion-limited kinetics. Therefore, the metamorphic heating timescale required to equilibrate phosphorus in meteoritic samples with small schreibersite grains (~1 μm), such as in the type 3 ordinary chondrites (3.0–3.3), was short (10–100 days).

1. Introduction

The element phosphorus (P) is a minor element in solar system solids. It has a cosmic abundance of about 0.007 phosphorus atoms per silicon atom (Anders and Grevesse, 1989) or about 926 ppm in CI chondrites (Wolf and Palme, 2001) and makes up about 0.17 % (10^{22} kg) of the total mass of the Earth (Smith, 1981; Nash, 1984; McDonough and Sun, 1995). Phosphorus is considered to be a moderately volatile element as it either dissolves in Fe-Ni metal or forms the iron-nickel phosphide mineral schreibersite, (Fe, Ni)$_3$P, at 1200 K, which is below the 1300 K condensation temperature of iron metal (Palme and Fegley, 1990). Notably, schreibersite is a solid solution with varying quantities of Ni in the M2 and M3 sites of the crystal lattice (Britvin et al., 2021). Phosphorus is thus generally believed to have condensed out of the solar nebula early into metal and/or phosphide (Pasek 2019b), as this solid solution. Once phosphorus formed phosphides, thermodynamic equilibrium models predict metal phosphides would have oxidized and transformed into phosphate minerals at temperatures between 300–800 K (Huss et al., 2006; Kimura et al., 2008, contrast to experiments below). These predictions generally fall within the context of the 'uniform' solar nebula, and a more dynamic solar nebula containing differing cooling

regimes would not significantly affect the major P species expected in the solar nebula. Even in a more dynamic solar nebula, most cosmochemists would consider only two phosphorus mineral systems in the solar system: lithophilic phosphates and siderophilic phosphides (Pirim et al., 2014).

In contrast to phosphates (with P^{5+}), P in phosphide minerals bears an oxidation state between 0 and −1 (Bryant et al., 2013; Pirim et al., 2014; La Cruz et al., 2016; Pasek et al., 2017, Bindi et al., 2023). Phosphide minerals readily react with water (including the extraction method used below) under a variety of conditions, producing several phosphorus oxyacid species that are illustrated in Fig. 1 (Pasek and Lauretta, 2005; Bryant and Kee, 2006; Pasek et al., 2007; Pantaleone et al., 2022). These phosphorus oxyacids form as the phosphide releases a phosphite radical (•PO_3^{2-}, species (h) in Fig. 1). For more details see Pasek et al. (2017) and Pasek (2019a). For this reason, these oxyacids or their oxyanions can be used to track the presence of phosphides during extraction of solid material.

Schreibersite is the most common phosphide mineral (Rubin and Ma, 2017,2021). It is frequently found in iron meteorites (Chabot et al., 2020; Gull et al., 2022), but is also present as a constituent of stony meteorites (Zolensky et al., 2002; Pasek, 2017) such as enstatite

---

* Corresponding author.
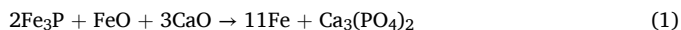 *E-mail address:* mpasek@usf.edu (M.A. Pasek).

chondrites (Pasek and Lauretta, 2008, Bsdok et al., 2020; Lin, 2022). Schreibersite can also be found in unequilibrated ordinary chondrites (type 3–3.3) where presumably the high temperatures required for oxidation did not occur (Huss et al., 2006; Rindlisbacher et al., 2021). The more oxidized phosphate minerals such as whitlockite, fluorapatite, and hydroxylapatite are usually more prevalent in equilibrated ordinary chondrites, carbonaceous meteorites and most stony achondrites (Nagy and Andersen, 1964; Fuchs, 1969). These minerals are usually in contact with silicates such as olivine and pyroxene, and occasionally calcic to sodic plagioclase. In chondrules phosphates are in contact with silicates such as pigeonite and augite, and glass, in the more volatile-poor chondrites (Rubin, 1997). Additional minerals such as metal, sulfides, and occasionally oxides are also often in direct contact with P-bearing phases.

Previous experiments reported that at high temperature (>1000 °C), schreibersite might sublimate within meteorite parent bodies in CO_2–H_2 gas mixtures, and at 800 °C it oxidizes, converting from schreibersite to graftonite ($Fe_3(PO_4)_2$) (Lauretta and Schmidt, 2009). Phosphide minerals might oxidize to calcium phosphate at low oxygen conditions over 1400 °C (Ikeda et al., 1997; Kirby et al., 2022). That is:

$$2Fe_3P + FeO + 3CaO \rightarrow 11Fe + Ca_3(PO_4)_2 \qquad (1)$$

This work investigates the oxidation of Fe_3P, a reasonable surrogate of schreibersite, in the presence of silicates at temperatures between 500 and 1000 °C to simulate metamorphic conditions in stony meteorites. This solid phase reaction may have occurred on meteorite parent bodies, where common silicate minerals and schreibersite would have been co-located, reacting to form calcium phosphates. In these experiments we use diopside as a Ca source, and though diopside is relatively uncommon in chondrites (Dunn et al., 2010), it has been used in prior experimental petrology studies (Friel and Goldstein, 1976; Olsen and Fuchs, 1967). Other Ca-bearing minerals may have instead served to promote phosphide oxidation (but would complicate the product mineralogy, especially for calcic plagioclase). We also note that phosphorus-rich olivine may exist as the intermediate phase in this oxidation. P-rich olivine has been found in the ungrouped carbonaceous chondrite Dar al Gani 978 (Li et al., 2017) and the LL chondrite Chelyabinsk (Walton et al., 2021). We envision such a reaction as potentially occurring within the well-mixed matrices of chondrites, especially ordinary chondrites. We tested a range of f_{O_2} conditions to identify how differing oxygen fugacity conditions (e.g., for carbonaceous vs. ordinary vs. enstatite chondrites) may alter the rate of phosphide oxidation.

2. Materials and methods

2.1. Materials

Forsterite (($Mg_{1.9}Fe_{0.1})SiO_4$, from Jackson County, NC, USA (Hunter et al., 1941)) and diopside ($CaMgSi_2O_6$, from Bird CK, Herschel, ON, Canada, (Satterly, 1977)) were purchased from Ward's Science, and their identities were confirmed by Laser Raman Spectroscopy and Powder XRD (Figure S1 and S2). Furthermore, to avoid phosphorus contamination in our experiment, both minerals were extracted using an Na_4EDTA solution (sodium ethylenediaminetetraacetate, described below) and the extract analyzed by ^{31}P NMR (nuclear magnetic resonance) spectroscopy to verify the absence of P as a major constituent.

In both prior work and our experiments below, Fe_3P is used instead of meteoritic schreibersite, $(Fe,Ni)_3P$, due both to the relative rarity of the schreibersite in meteoritic samples, and the availability of iron phosphide as Fe_3P, which is crystallographically identical to schreibersite and is the major natural form of schreibersite in terrestrial samples (e.g., Hess et al., 2021; Bindi et al., 2023). For this reason, most chemical reactions use "Fe_3P" as schreibersite, as this keeps reaction stoichiometry simple by considering only the iron end-member of schreibersite.

Sodium hydroxide (NaOH, 98.5%, 500g) and deuterated water (D_2O, 99.8 atom %, 100 ml) were purchased from Acros Organics. EDTA acid powder (99.5 %, 500g) was purchased from Sigma-Aldrich. Iron phosphide (Fe_3P, 99.5 %) and sodium sulfide nonahydrate ($Na_2S\cdot9H_2O$, 98 %) were purchased from Thermo Scientific. ^{18}O water ($H_2^{18}O$, 99 % atom %) was from Cambridge Isotope Laboratories, Inc. Industrial grade argon gas (99.997 %, CGA-500) was bought from Airgas. Deionized water (DI H_2O) was purified in house using a Barnstead (Dubuque, IA, USA) NANO pure® Diamond Analytical combined reverse osmosis-deionization system (Gull et al., 2020; Feng et al., 2021).

2.2. Methods

Forsterite and diopside were powdered by a mineral grinder, resulting in a median grain size of 10 μm as measured by a digital microscope. The mineral powders were then mixed with Fe_3P (with a median grain size of 4 μm) in a small alumina assay crucible (50 mm × 20 mm × 20 mm) with a molar ratio of 10 Mg_2SiO_4: 10 $CaMgSi_2O_6$: 1 Fe_3P, and a total mass of 2.00 g. To minimize pore space, the mineral powder mixtures were pressed into a pellet before being placed inside the crucible. Then the smaller crucible was placed upside down within a larger alumina assay crucible (100 mm × 40 mm × 20 mm) and
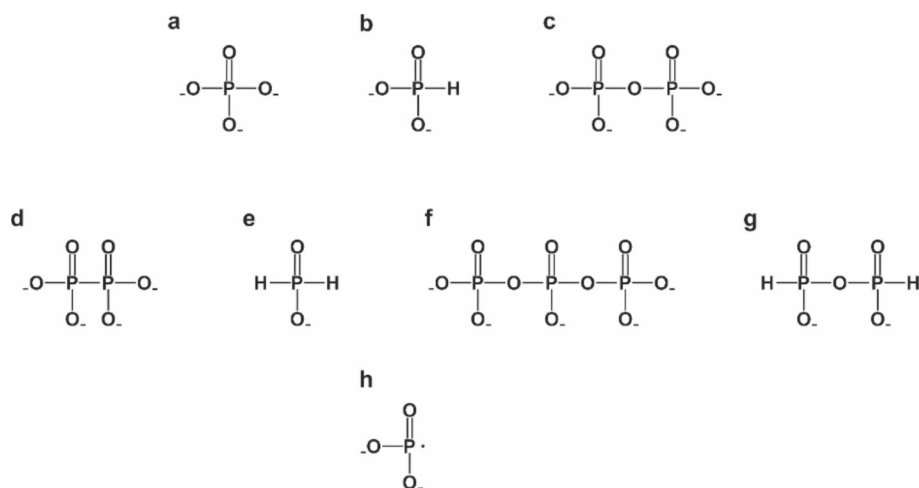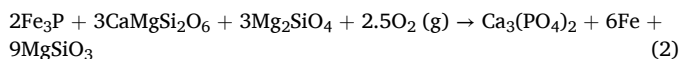

Fig. 1. Structures of conjugate bases of phosphorus oxyacids that are discussed in this research. a) Orthophosphate (PO_4^{3-}). b) Phosphite (HPO_3^{2-}). c) Pyrophosphate ($P_2O_7^{4-}$). d) Hypophosphate ($P_2O_6^{4-}$). e) Hypophosphite ($H_2PO_2^{-}$). f) Triphosphate ($P_3O_{10}^{5-}$). g) Pyrophosphite ($H_2P_2O_5^{2-}$). h) Radical phosphite (• PO_3^{2-}). c) and f) are often grouped together as "polyphosphates" or "poly-P".

surrounded with a mineral redox buffer to control the oxygen fugacity during the heating experiments. The internal crucible had a small gap at its edge to allow oxygen to transfer between the mineral pellet and the outside buffer (Figure S3). Four types of mineral redox buffers were used in the larger crucible, including: (i) Magnetite-Hematite buffer (molar ratio 1:1, shown as MH); (ii) Iron-Magnetite buffer A (molar ratio 1:1, shown as IM-A); (iii) Iron-Magnetite buffer B (molar ratio 4:1, similar to an Iron-Wüstite buffer, shown as IM-B) and (iv) a Silicon-Silica buffer (molar ratio 1:1, shown as SS). In each experiment over 20.00 g of buffer were used. The reaction expected to occur within the interior experimental mineral powder (labeled as Sch-Fo-Dio,) was:

$$2Fe_3P + 3CaMgSi_2O_6 + 3Mg_2SiO_4 + 2.5O_2(g) \rightarrow Ca_3(PO_4)_2 + 6Fe + 9MgSiO_3 \tag{2}$$

The sample and buffer crucibles were placed together into a horizontal tube furnace housed at USF. Before heating, the furnace tube was filled with argon gas and flushed three times at room temperature to generate and retain anoxic conditions. The mineral samples were heated to 500 °C, 600 °C, 700 °C, 800 °C, 900 °C and 1000 °C for 6 h, 12 h, 24 h and 120 h. Each heating experiment was run with each of the four mineral redox buffers, and a total of 96 products were collected in the first series of experiments (La Cruz et al., 2016; Feng et al., 2021). A Thermo Scientific Lindberg Blue M HTF55000 Series Hinged Tube Furnace was controlled by CC58114A (120V/11A/1330W), which can ramp from room temperature to 1100 °C in 20 min.

Due to possible grain size effects on the Fe_3P oxidation rate, the minerals' grain sizes were investigated with a Keyence VHX − 7000 digital microscope prior to heating. Grain size measurements were collected using quick composition and 3D image stitching. Multiple grains (Fe_3P, forsterite and diopside) were chosen to measure the long axis profile. This was done by a 2-point line from rim to rim. The 2-point line measurements record the length and height. Images were taken between 150 and 300× magnification.

After heating, all the sample products were removed from the furnace and the solids were analyzed by powder X-ray diffractometry (XRD) and laser Raman Spectroscopy, and aqueous extracts were analyzed by ^{31}P NMR. A subset of the solids was analyzed by X-Ray Photoelectron Spectroscopy (XPS) and Scanning Electron Microscopy (SEM).

An Enwave Opt. Inc. (Model No. EZI-785-A2) laser Raman spectrometer was utilized to determine the initial major mineral component before and after the heating experiments following previous work (Feng et al., 2019; Gull et al., 2023). Crystal Sleuth software was used for mineral ID, employing the RRUFF database reference (Laetsch and Downs, 2006). A Bruker D8 Advance powder X-ray diffractometer (University of South Florida) was used to investigate how Fe_3P in the sample changed during heating. Analysis of the surface oxidation state was performed on a Thermo K-alpha analytical XPS system at the Georgia Institute of Technology. The data were collected under ultrahigh vacuum conditions ($\sim 10^{-9}$ Torr) using an X-ray spot size of 400 µm (Pirim et al., 2014; Schaible et al., 2019), and data were collected after ion sputtering of surfaces (removing 10–20 nm of material). SEM measurements were carried out at Florida International University using a JEOL JSM 5900 Scanning Electron Microscope. Compositions were quantified using Energy Dispersive X-ray Spectrometry via a Bruker-Quantax-SDD-EDS.

To further investigate the P specification, all sample products were analyzed by ^{31}P − NMR. To avoid the influence of iron ions, which prevents accurate NMR acquisition, 0.1 g of each experiment (a solid powder) was extracted with a sodium hydroxide-EDTA solution (Na_4EDTA, 0.05M, 10 ml, pH=13) for one week. This extraction method efficiently binds iron, extracts P species from the sample, and does not contaminate P speciation (Turner et al., 2003; Pasek et al., 2022). Then, the extracted solution was filtered and air-dried at room temperature in a watch glass. The dried extract was then rehydrated with 0.5 ml of D_2O

to enable analysis by ^{31}P − NMR.

In addition, extraction in $H_2^{18}O$ was performed on a subset of these samples to examine the origin of O in the P species (whether from the silicates, air, or water). In this work, two samples (800 °C temperatures-24h reaction time- MH buffer; 800 °C temperatures – 24h reaction time-IM-A buffer) were selected as target samples. These two sample products (0.1 g) were first mixed with $H_2^{18}O$ (1.0 g, 99 % ^{18}O) for 60 days as in previous research (Bryant and Kee, 2006), then extracted in a sodium sulfide-EDTA solution (Na_4EDTA, 0.05M, 10ml, pH=13) for one week. These two solutions were dried and rehydrated with D_2O for ^{31}P − NMR analysis.

The ^{1}H-coupled ^{31}P − NMR was run on a Bruker Neo 600 MHz NMR spectrometer. Every sample was run for 6000 normal scans at 242.86 MHz with a 0.34 s delay between acquisitions. The running temperature was at 298K (25°C) (Herschy et al., 2018; Lago et al., 2020; Omran et al., 2022).

3. Results

3.1. Mineral changes during thermal oxidation

Powder XRD (Fig. 2) and XPS (Fig. 3) show that the samples significantly changed after heating. Specifically, in the XRD analysis, the peaks corresponding to schreibersite vanish completely at 1000 °C in the diffractograms. Both forsteritic olivine and diopside were present in samples after heating, implying both minerals remained, though schreibersite was lost to oxidation.

Oxidation of schreibersite results in the development of phosphate. The XPS results demonstrate that peaks corresponding to phosphorus in a +5 phosphate oxidation state develop when temperatures were elevated over 800 °C for P-bearing phases. These peaks in contrast are absent at temperatures of 500 °C (Fig. 3). The XPS data suggest that oxidation on the surface of P-bearing phases has begun by 800 °C with an initial P $2p^{3/2}$ peak position at 133.8 eV (the $2p^{3/2}$ and $2p^{1/2}$ peak separation was fixed at 2.2 eV). Oxidation at 1000 °C causes the peaks to shift to slightly lower binding energy. Notably, this oxidation is more frequently seen on the Fe of schreibersite then the P.

The SEM results (Figure S4) show that after thermal oxidation, P was not associated with Fe, but instead associated with Ca. This indicates
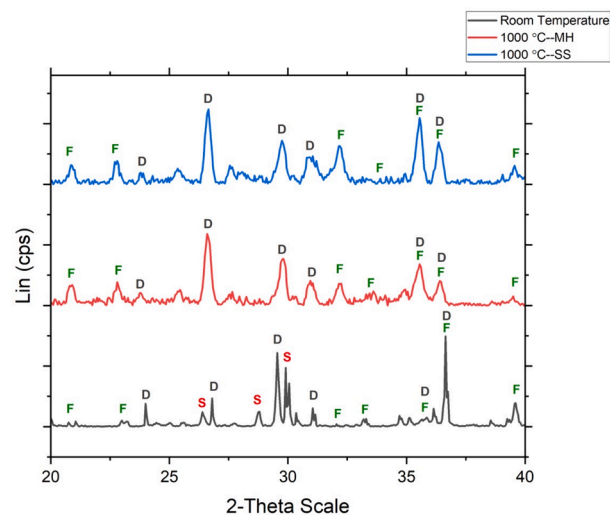

Fig. 2. Powder X-ray diffraction pattern for samples heated under argon. The bottom is room temperature (black), middle is 1000 °C with MH buffer (red) and top is 1000 °C with SS buffer (blue). Each reaction was run for 24 h. Forsterite (expressed by olive color **F**) and diopside (expressed by dark grey color **D**) are both stable at room temperature conditions and at 1000 °C. However, the schreibersite (expressed by red color **S**) peaks disappeared at 1000 °C under both the MH buffer and SS buffer.
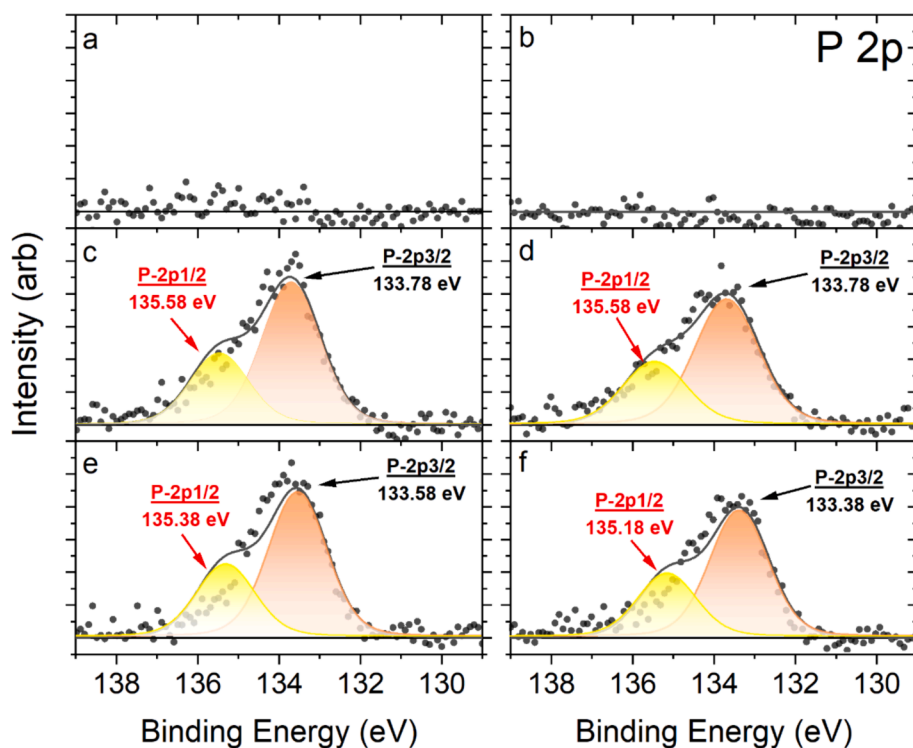
Fig. 3. High-resolution X-ray photoelectron spectra of the P (2p) level in Fe$_3$P thermal oxidation products after 3 kV Ar$^+$ etching (for 120 s). a) Fe$_3$P oxidation in the IM-A mineral buffer at 500 °C, b) with IM-B mineral buffer at 500 °C, c) with IM-A mineral buffer at 800 °C, d) with IM-B mineral buffer at 800 °C, e) with IM-A mineral buffer at 1000 °C, and f) with IM-B mineral buffer at 1000 °C.

that after heating, the majority of iron phosphide has transformed into Ca phosphate minerals and is not present as either iron phosphide or phosphate minerals.

^{31}P NMR provides a bulk analysis of all P speciation in samples. NMR results are shown in Fig. 4 and reveal the P species in these oxidation experiments varies significantly as a function of temperature, heating timescale, and oxygen fugacity. Reduced P species (hypophosphite, phosphite, and pyrophosphite) dominate at low temperatures (500 °C
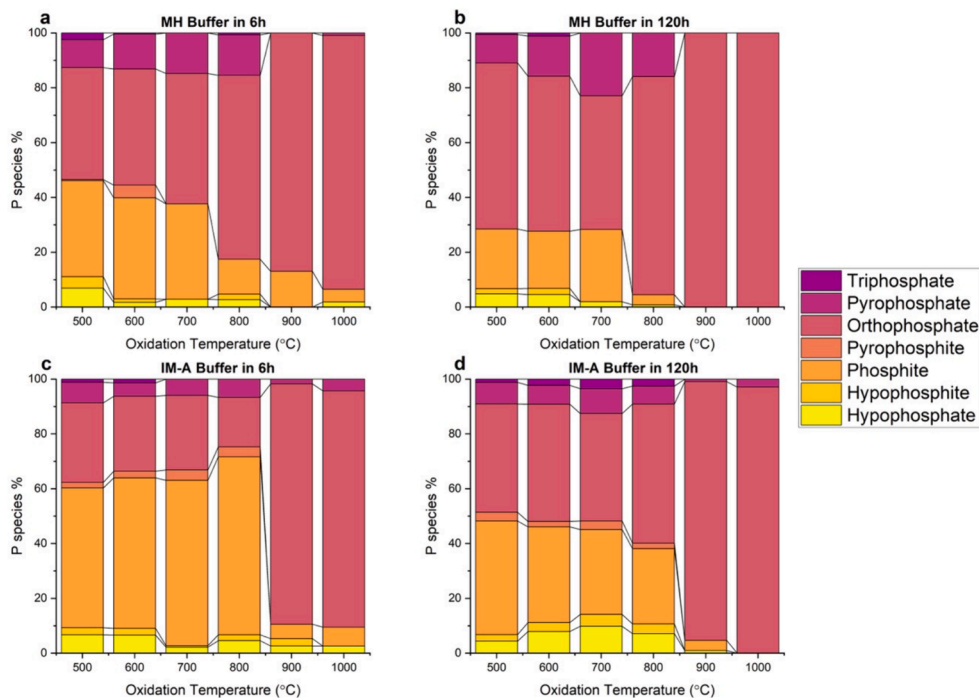

Fig. 4. Fraction of phosphorus species (percent) from schreibersite thermal oxidation experiments under argon. These data were collected using ^{1}H coupled ^{31}P NMR analysis (spectra acquired at 242.86 MHz and with an extraction at pH 13). a). Schreibersite oxidation with MH buffer for 6 h. b). Schreibersite oxidation with MH buffer for 120 h. c). Schreibersite oxidation with IM-A buffer for 6 h. d). Schreibersite oxidation with IM-A buffer for 120 h.

and 600 °C), at short timescales (< 24h), and in low oxygen fugacity environments. For reaction temperatures 900 °C and above, the reduced P species were mostly converted into phosphate (P^{+5}) species. For example, Fig. 4 shows the conversion of P species such as phosphite into phosphate as temperatures increase (see also Figure S5, S8, S9, S12).

The presence of reduced P species in these experiments is expected based on XRD, XPS, and SEM results, which all show that iron phosphide is present under short, low-temperature, and reduced conditions. In extraction experiments, the presence of both hypophosphate ($P_2O_6^{4-}$, P^{4+}) and phosphite (HPO_3^{2-}, P^{3+}) are used as indicators of the presence of iron phosphide (see Introduction).

3.2. Sample examination with ^{18}O

For the calculations that follow, we assume that P species of lower redox than phosphate (P^{5+}) must have originated from iron phosphide. In contrast, phosphate and polyphosphate may have been generated both from extraction of phosphate and from iron phosphide. In general, iron phosphide oxidizes to phosphate and phosphite (1:1), and hypophosphate and pyrophosphate (0.15:0.15, Pasek et al., 2007). Therefore, NMR spectra that show phosphate and phosphite at a roughly 1:1 ratio are expected to have extracted P from iron phosphide, whereas those that have more orthophosphates will have extracted P from phosphate in addition to iron phosphide.

To verify this chemical assumption (that low redox P comes from iron phosphide), we extracted two samples (800 °C–24h–MH; 800 °C–24h–IM-A) with isotopically labelled water ($H_2^{18}O$). Our results indicate that both orthophosphate and phosphite are shifted upfield about 0.08ppm (Fig. 5, Table S1). This result is consistent with isotopic experiments by Bryant and Kee (2006) where each P species was shifted by 0.077ppm. Bryant and Kee (2006) argued that a single replacement of ^{16}O with ^{18}O causes peaks to shift by 0.02 ppm, thus implying an incorporation of at least three ^{18}O atoms in both molecules (Sorensen-Stowell and Hengge, 2005).

For all experiments, the presence of adventitious ^{16}O results in the presence of a ^{16}O-only phosphorus oxyacid peak. Bryant and Kee (2006) attribute adventitious ^{16}O to trace atmospheric oxidation in the powder, but in these experiments it may also have originated from the neighboring silicates. These results are consistent with Pasek et al. (2007)'s argument that Fe₃P releases $\cdot PO_3^{2-}$ radicals upon reaction with water, which in these experiments would have been completely $P^{18}O_3^{2-}$. However, the two isotopically-labeled extractions differ in peak heights of the phosphates. In Fig. 5(a), which was done under the magnetite-hematite buffer, the peak corresponding to ^{16}O-phosphate is more significant than the ^{18}O phosphate peak. In contrast, under the Fe-Fe₃O₄ (IM-A) buffer, the peak corresponding to ^{18}O phosphate is more significant than the ^{16}O phosphate peak, indicating that the O in the phosphate was sourced primarily from extracting solution. In both cases the ^{18}O phosphite peaks are larger than the ^{16}O phosphite peaks, indicating

that the production of phosphite in these experiments comes from the ^{18}O-labeled water reacting with iron phosphide.

4. Discussion

The phosphides are expected to dominate under reduced conditions, whereas the phosphates should dominate under more oxidizing conditions (Olsen and Fuchs, 1967, see Fig. 6). Our experiments are broadly consistent with these findings; the rate of oxidation is slower at lower temperature, and with lower oxygen fugacity, there is less of a thermodynamic driver for the oxidation of phosphides. The reducing conditions would have been present in the higher temperature material in the early protoplanetary disk (based on condensation calculations), and the oxidizing conditions would have dominated as this reduced material cooled and mixed with more oxidizing material (Lewis, 1972) such as water. This work explored the transition in solid state between phosphides and phosphates, identifying the timescale of this reaction as a function of temperature, time, and oxygen fugacity.

4.1. Schreibersite oxidation conditions

These experiments indicate schreibersite is overall unstable in chondrites that reached T > 500 °C (e.g., thermally altered as opposed to aqueously altered chondrites). The final product of schreibersite
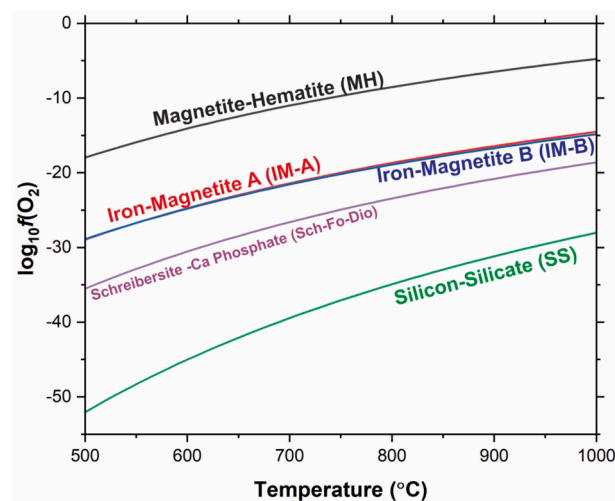
Fig. 6. Mineral redox buffers plotted along with the schreibersite-silicate reaction (Sch-Fo-Dio, purple color). The buffers are Magnetite-Hematite (MH, black color), Iron-Magnetite A (IM-A, ratio 1:1, red color), Iron-Magnetite B (IM-B, ratio 4:1, blue color), and Silicon-Silicate (SS, green color). Data was selected from HSC Chemistry (version 6, Outokumpu Research Oy).
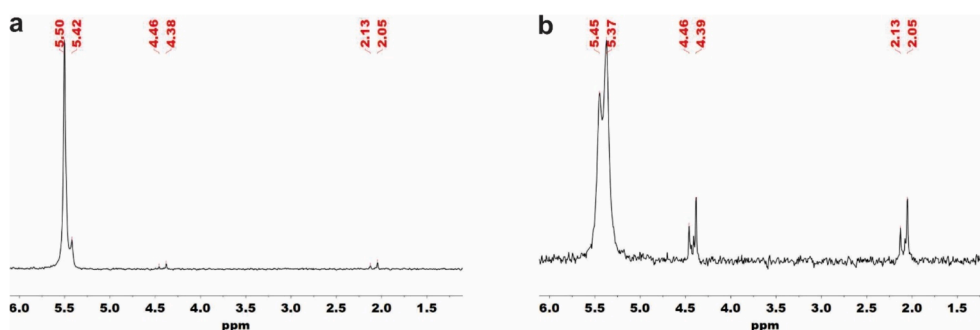
Fig. 5. ^1H coupled ^{31}P NMR spectra for iron phosphide oxidation experiments extracted with $H_2^{18}O$. The ^{18}O-labelled peaks occur upfield (to the right) of the ^{16}O peaks. The ^{31}P NMR spectra was collected in D_2O, at 161.8 MHz and at pH 13. a). Extraction of the mixture under MH buffer heated at 800 °C for 24 h. b) Extraction of the mixture under with IM-A buffer heated at 800 °C for 24 h.

oxidation in these conditions is calcium phosphate (Figure S4), and this phase forms from the solid-state reaction with silicate minerals, including olivine and diopside in chondrite parent bodies.

Fig. 6 shows the relation between oxygen fugacity and reaction temperature for iron phosphide reacting with forsterite and diopside (equation (2)), which is what is expected at equilibrium. This chemistry suggests that at high temperatures, schreibersite transforms into calcium phosphate through a solid-state reaction with silicate minerals (Fig. 6), ignoring kinetic factors. As temperature increases, the products of schreibersite oxidation also changed. Generally, phosphates are abundant under oxygen-sufficient conditions (Fig. 7a). However, reduced and poly-P species (Fig. 1) are also present in the product distribution of these extracts. These P species are influenced by the temperature of schreibersite oxidation, oxidation time and oxygen buffer. These three factors are all positively correlated with phosphate percentage, with higher temperature, longer reaction times, and more oxidizing conditions favoring more orthophosphate in the extracts.

The temperature is the primary factor that influences P speciation in the thermal reactions described here. At lower reaction temperatures (under 900 °C), P oxidation states are diverse (in that the average oxidation state is not just P^{5+}) in all experiments, even with long reaction times and an oxygen-rich buffer (MH, Fig. 7(a)). On the other hand, when the temperature was over 900 °C, over 90 % of all P was in orthophosphate, and the oxidation time and oxygen fugacity had very little effect on the P species diversity in the product distribution (Fig. 7, Figure S5-S20, Table S2-S5).

The current work shows that iron phosphide begins to oxidize at temperatures as low as 800°C under all f_{O2} with a timescale of hours. Specifically, powder XRD results show that iron phosphide reacts completely at high temperature (900–1000 °C), and XPS results show phosphide surfaces oxidize to phosphate beginning at 800°C. Moreover, SEM results show iron phosphide oxidizes in the presence of Ca-bearing phases to form Ca-phosphates, not iron phosphates, indicating

scavenging of Ca during phosphide oxidation. Bulk analysis by ^{31}P NMR indicates that iron phosphide oxidation occurs gradually over a range of time and temperature conditions, for different f_{O2}. Connecting this back to chondritic meteorites (specifically those that experienced primarily thermal alteration, e.g., the ordinary chondrites), schreibersite should similarly react completely on short timescales.

4.2. Rates of schreibersite oxidation

Iron phosphide is extracted under our experimental setup to afford a mixed valence set of phosphorus oxyacids: phosphite, phosphate, hypophosphate, and pyrophosphate. We find the average oxidation state of P in extracts of iron phosphide is typically between 3–4. In Gull et al. (2022), the authors report reduced species as being present in extracts of iron phosphide that had been submerged in water for eight years. In contrast to this long extraction timescale, the extraction timescale we use was much shorter (8 weeks at most for the ^{18}O-labeled water extractions). Therefore, these ions should be representative of the minerals being extracted, provided there is no further oxidation.

Pasek and Lauretta (2005) and Pasek et al. (2007) both report one additional oxidation route for the ion phosphite (HPO_3^{2-}) that occurs during extraction in aqueous solution. In the presence of iron metal (but not silicates, silicon, or iron oxides), phosphite can oxidize to phosphate. It does so because iron metal reacts with O_2 from the air, reducing it to H_2O_2 upon reaction with water, which then reacts with Fe^{2+} to generate hydroxyl radicals. The reaction of OH radicals with phosphite produces phosphate in an oxidation reaction (Pasek et al., 2008). Therefore, in our experiments that utilize iron metal (IM-A, IM-B), we expect some phosphite to be lost during extraction under air.

We determine the rate of oxidation of Fe_3P as a function of temperature, time, and oxygen fugacity. This is done using solid state kinetic models (e.g., Khawam and Flanagan, 2006). Specifically, the average oxidation state of the P species observed in solution was taken to reflect
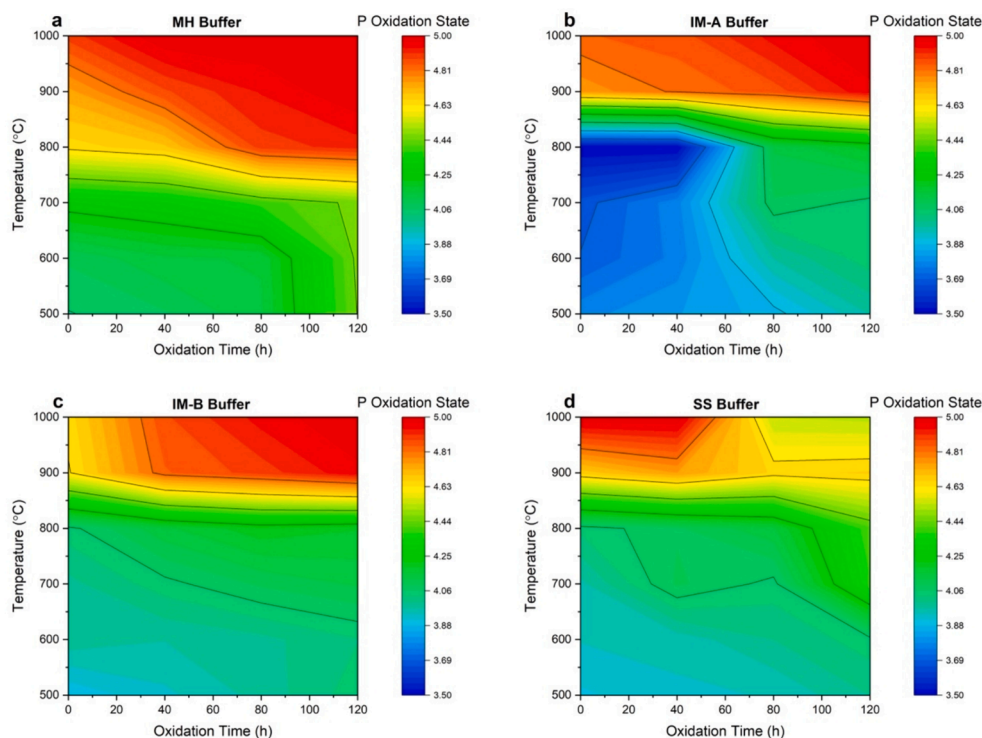

Fig. 7. The average oxidation state of phosphorus species in the extracts as a function of temperature and time. Data was collected by ^{1}H coupled ^{31}P NMR spectra and calculated by such function: Total charge = (P^{5+} total percent) × 5 + (P^{3+} total percent) × 3 + (P^{4+} total percent) × 4 + (P^{1+} total percent) × 1, to give a weighted average oxidation state. a). Iron phosphide oxidation with MH buffer. b). Iron phosphide oxidation with IM-A buffer. c). Iron phosphide oxidation with IM-B buffer. d). Iron phosphide oxidation with SS buffer.

the reaction conversion fraction (α), which is given as equation (3):

$$\alpha = \frac{R_0 - R_t}{R_0 - R_\infty} \qquad (3)$$

where R_0 is the weighted average redox state at time zero, R_t is the weighted average redox state at time (t), and R_∞ is the final weighted average redox state (+5). Notably, the rate of change of α (dα/dt) is related to the Arrhenius equation by equation (4):

$$\frac{d\alpha}{dt} = Ae^{\left(-\frac{Ea}{RT}\right)}f(\alpha) \qquad (4)$$

where A is the preexponential factor, Ea is the activation energy, R is the gas constant, T is the temperature in Kelvin, and f(α) is the reaction model. We tested several reaction models (e.g., Khawam and Flanagan, 2006) and found that the 3D diffusion models, specifically the Ginstling-Brounshtein equation (1950), which is equation (5) worked the best at giving a specific reaction rate k at a given temperature:

$$f(\alpha) = \frac{1}{k} \cdot \frac{d\alpha}{dt} = \frac{3}{2(1-\alpha)^{\left(-\frac{1}{3}\right)} - 1} \qquad (5)$$

From this, the relationship of $\ln\left(\frac{d\alpha}{dt} \cdot \frac{1}{f(\alpha)}\right)$ vs. 1/T affords the activation energy as the slope × −R.

We derive an activation energy of 83 ± 8 kJ/mol for all four buffers (Fig. 8). The buffers differ in terms of slope-intercept (equal to the value ln[A]), by values of about 1.62 for the MH to the IM to the SS buffers each, implying the MH buffer is about 5× faster than the IM buffers, which itself is 5× faster than the SS buffer with respect to oxidation. The oxidation rate of Fe_3P is primarily influenced by the slow diffusion of oxygen to Fe_3P, which results in its oxidation to phosphate.

From these kinetic results we estimate that schreibersite oxidizes on the timescale of hours to weeks under our experimental conditions, and that this timescale is dependent on both temperature and oxygen fugacity. From our derived activation energy, we estimate that at lower temperatures (~500 °C), oxidation would be 100-1000× slower than at 1000°C. Notably, if the rate of reaction is proportional to grain size (as would be the case for being diffusion-controlled), then the timescale for a reaction is proportional to size squared. Given that the rate of this oxidation is proportional to the square of the size of the grains (and that ours are ~3 μm), grains that are ~ 1 mm in size would be expected to oxidize on timescales of the order of 10,000 years, depending on the temperature (for example at 900 °C) and f_{O2} (at the iron-magnetite buffer). Grains that are ~cm in size should oxidize over 10^6 years (under similar conditions). Porosity and grain surface diffusion may play a larger role in phosphide oxidation, as this may shift kinetics away from diffusion-limited to grain-boundary-limited, with decreasing porosity favoring diffusion-limited kinetics. In our experiments, the powders were pressed into a pellet prior to being heated. However, for a more porous object (such as a rubble pile asteroid), porosity would likely play a role in the oxidation reaction rates of phosphides.

We also note that schreibersite in most meteorites is more nickel-rich. This may slow the oxidation of meteoritic schreibersite as nickel is more 'noble' than iron, and hence may be less susceptible to oxidation. However, given the relative ease of oxidation even under the Si-SiO_2 buffer, the effect of Ni in the phosphide is likely smaller than the effect of temperature and hence oxidation is still likely under short timescales even with nickeliferous schreibersite.

5. Conclusion

In this work, we focus on the thermal oxidation of schreibersite in meteorites. In ordinary chondrites, schreibersite is absent in those chondrites that are type 3.3 and above. From our results, this is likely
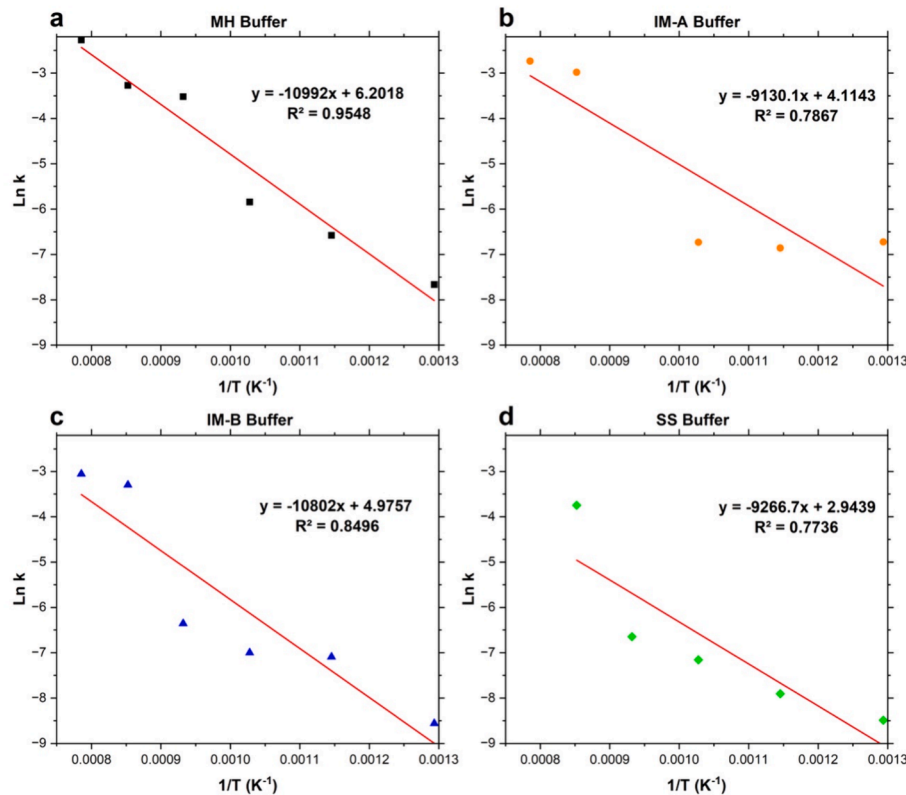

Fig. 8. Diagram for the relation between reciprocal of temperature of iron phosphide thermal oxidation (1/T) and natural logarithm of the rate constant. a). Iron phosphide oxidation with MH buffer. b). Iron phosphide oxidation with IM-A buffer. c). Iron phosphide oxidation with IM-B buffer. d). Iron phosphide oxidation with SS buffer.

because these chondrites were heated for a sufficient amount of time to cause all phosphides to convert to phosphates. For ordinary chondrites, which experienced depth-dependent heating with maximum temperatures exceeding 800 °C for up to a few tens of millions of years (generally believed to be from radiogenic decay, see Henke et al., 2012, Gail and Trieloff, 2019), all schreibersite (~0.1 mm) would be expected to be oxidized at depth under such conditions. To this end, the chemistry of phosphorus within equilibrated chondrites would be expected to be completely phosphate, as confirmed from meteoritic observations.

In contrast, were there meteorite parent bodies with schreibersite grains with sizes of ~1 cm in a mix of silicates, then complete loss of phosphides may not have occurred even if subjected to longer heating timescales. To this end, schreibersite and its oxidation products can be used to infer peak temperatures especially if co-occurring with Ca-phases, as part of a larger suite of mineral reactions with time- and condition-dependent rates.

Data Availability

Data are available through ResearchGate at DOI: 10.13140/RG.2 .2.22646.37448.

CRediT authorship contribution statement

Tian Feng: Conceptualization, Formal analysis, Investigation, Methodology, Resources, Visualization, Writing – original draft, Writing – review & editing. **Arthur Omran:** Writing – original draft. **Maheen Gull:** Writing – original draft. **Micah J. Schaible:** Formal analysis, Visualization, Writing – original draft. **Thomas M. Orlando:** Methodology, Writing – original draft. **Matthew A. Pasek:** Conceptualization, Formal analysis, Funding acquisition, Investigation, Methodology, Resources, Software, Supervision, Validation, Visualization, Writing – original draft, Writing – review & editing.

Declaration of competing interest

The authors declare that they have no known competing financial interests or personal relationships that could have appeared to influence the work reported in this paper.

Acknowledgements

Appendix A. Supplementary material

Supplementary materials include Raman and XRD of precursor material, diagram of experimental setup, SEM mapping of material after reaction, and copies of all NMR data in both figure and table form. Supplementary material to this article can be found online at https://doi.org/10.1016/j.gca.2024.07.022.

References

Anders, E., Grevesse, N., 1989. Abundances of the elements: meteoritic and solar. Geochim. Cosmochim. Acta 53, 197–214.

Bindi, L., Feng, T., Pasek, M.A., 2023. Routes to reduction of phosphate by high-energy events. Commun. Earth Environ. 4, 70.

Britvin, S.N., Krzhizhanovskaya, M.G., Zolotarev, A.A., Gorelova, L.A., Obolonskaya, E. V., Vlasenko, N.S., Shilovskikh, V.V., Murashko, M.N., 2021. Crystal chemistry of schreibersite,(Fe, Ni) $_3$P. Am. Mineral. 106, 1520–1529.

Bryant, D.E., Kee, T.P., 2006. Direct evidence for the availability of reactive, water soluble phosphorus on the early Earth. H-Phosphinic acid from the Nantan meteorite. Chem. Commun. (Camb) 22, 2344–2346.

Bryant, D.E., Greenfield, D., Walshaw, R.D., Johnson, B.R., Herschy, B., Smith, C., Pasek, M.A., Telford, R., Scowen, I., Munshi, T., Edwards, H.G.M., Cousins, C.R., Crawford, I.A., Kee, T.P., 2013. Hydrothermal modification of the Sikhote-Alin iron meteorite under low pH geothermal environments. A plausibly prebiotic route to activated phosphorus on the early Earth. Geochim. Cosmochim. Acta 109, 90–112.

Bsdok, B., Altenberger, U., Concha-Perdomo, A.E., Wilke, F.D.H., Gil-Rodríguez, J.G., 2020. The Santa Rosa de Viterbo meteorite, Colombia. New work on it's petrological, geochemical and economical characterization. J. South Am. Earth Sci., 102779

Chabot, N.L., Cueva, R.H., Beck, A.W., Ash, R.D., 2020. Experimental partitioning of trace elements into schreibersite with applications to IIG iron meteorites. Meteorit Planet Sci. 55, 726–743.

Dunn, T.L., McCoy, T.J., Sunshine, J.M., McSween Jr, H.Y., 2010. A coordinated spectral, mineralogical, and compositional study of ordinary chondrites. Icarus 208, 789–797.

Feng, T., Lang, C., Pasek, M.A., 2019. The origin of blue coloration in a fulgurite from Marquette, Michigan. Lithos 342, 288–294.

Feng, T., Gull, M., Omran, A., Abbott-Lyon, H., Pasek, M.A., 2021. Evolution of ephemeral phosphate minerals on planetary environments. ACS Earth Space Chem. 5, 1647–1656.

Friel, J.J., Goldstein, J.I., 1976. An experimental study of phosphate reduction and phosphorus-bearing lunar metal particles. In: Proc. 7Th Lunar Sci. Conf. 7. Pergamon Press, New York, pp. 791–806.

Fuchs, L.H., 1969. The phosphate mineralogy of meteorites. In: Millman, P. (Ed), Meteorite Research: Proceedings of a Symposium on Meteorite Research Held in Vienna, Austria, 7–13 August 1968. Springer, Netherlands, pp. 683–695.

Gail, H.P., Trieloff, M., 2019. Thermal history modelling of the L chondrite parent body. Astron. Astrophys. 628, A77.

Ginstling, A.M., Brounshtein, B.I., 1950. Concerning the diffusion kinetics of reactions in spherical particles. J. Appl. Chem. USSR 23, 1327–1338.

Gull, M., Omran, A., Feng, T., Pasek, M.A., 2020. Silicate-, magnesium ion-, and urea-induced prebiotic phosphorylation of uridine via pyrophosphate; revisiting the hot drying water pool scenario. Life (Basel) 10, 122.

Gull, M., Feng, T., Pasek, M.A., 2022. Results of an eight-year extraction of phosphorus minerals within the Seymchan Meteorite. Life (Basel) 12, 1591.

Gull, M., Feng, T., Bracegirdle, J., Abbott-Lyon, H., Pasek, M.A., 2023. Organophosphorus compound formation through the oxidation of reduced oxidation state phosphorus compounds on the hadean earth. J. Mol. Evol. 91, 60–75.

Henke, S., Gail, H.P., Trieloff, M., Schwarz, W.H., Kleine, T., 2012. Thermal evolution and sintering of chondritic planetesimals. Astron. Astrophys. 537, A45.

Herschy, B., Chang, S.J., Blake, R., Lepland, A., Abbott-Lyon, H., Sampson, J., Atlas, Z.D., Kee, T.P., Pasek, M.A., 2018. Archean phosphorus liberation induced by iron redox geochemistry. Nat. Commu. 9, 1–7.

Hess, B.L., Piazolo, S., Harvey, J., 2021. Lightning strikes as a major facilitator of prebiotic phosphorus reduction on early Earth. Nat. Commu. 12, 1535.

Hunter, C.E., Tennessee Valley Authority, Rankin, H.S., 1941, Forsterite olivine deposits of North Carolina and Georgia. North Carolina. Department of Conservation and Development, pp. 117.

Huss, G.R., Rubin, A.E., Grossman, J.N., 2006. Thermal metamorphism in chondrites. In: Lauretta, D.S., McSween, H.Y. (Eds.), Meteorites and the Early Solar System II. University of Arizona Press, Tucson, pp. 567–586.

Ikeda, Y., Ebihara, M., Prinz, M., 1997. Petrology and chemistry of the Miles IIE iron. I: Description and petrology of twenty new silicate inclusions. Antarct. Meteorite. Res. 10, 355.

Khawam, A., Flanagan, D.R., 2006. Solid-state kinetic models: basics and mathematical fundamentals. J. Phys. Chem. B 110, 17315–17328.

Kimura, M., Grossman, J.N., Weisberg, M.K., 2008. Fe-Ni metal in primitive chondrites: Indicators of classification and metamorphic conditions for ordinary and CO chondrites. Meteorit. Planet. Sci. 43, 1161–1177.

Kirby, R.S., King, P.L., Norman, M.D., Ireland, T.R., Forster, M., Pelton, A.D., Troitzsch, U., Tamura, N., 2022. Formation, cooling history and age of impact events on the IIE iron parent body: evidence from the Miles meteorite. Geochim. Cosmochim. Acta 339, 157–172.

La Cruz, N.L., Qasim, D., Abbott-Lyon, H., Pirim, C., McKee, A.D., Orlando, T., Gull, M., Lindsay, D., Pasek, M.A., 2016. The evolution of the surface of the mineral schreibersite in prebiotic chemistry. Phys. Chem. Chem. Phys. 18, 20160–20167.

Laetsch, T., Downs, R.T., 2006. Software for Identification and Refinement of Cell Parameters from Powder Diffraction Data of Minerals Using the RRUFF Project and American Mineralogist Crystal Structure Databases. In: 19th General Meeting of the International Mineralogical Association, Kobe, Japan, Vol. 23, p. e28.

Lago, J.L., Burcar, B.T., Hud, N.V., Febrian, R., Mehta, C., Bracher, P.J., Atlas, Z.D., Pasek, M.A., 2020. The prebiotic provenance of semi-aqueous solvents. Orig. Life. Evol. Biosph. 50, 1–14.

Lauretta, D.S., Schmidt, B.E., 2009. Oxidation of minor elements from an iron–nickel–chromium–cobalt–phosphorus alloy in 17.3% CO_2–H_2 gas mixtures at 700–1000 °C. Oxid. Met. 71, 219–235.

Lewis, J.S., 1972. Low temperature condensation from the solar nebula. Icarus 16, 241–252.

Li, Y., Zhang, A.C., Chen, J.N., Gu, L.X., Wang, R.C., 2017. Formation of phosphorus-rich olivine in Dar al Gani 978 carbonaceous chondrite through fluid-assisted metamorphism. Am. Mineral. 102, 98–107.

Lin, Y., 2022. Enstatite chondrites: condensation and metamorphism under extremely reducing conditions and contributions to the Earth. Prog. Earth Planet Sci. 9, 1–16.

McDonough, W.F., Sun, S.S., 1995. The composition of the Earth. Chem. Geol. 120, 223–253.

Nagy, B., Andersen, C.A., 1964. Electron probe microanalysis of some carbonate, sulfate and phosphate minerals in the Orgueil meteorite. Am. Mineral. 49, 1730–1736.

Nash, W.P., 1984. Phosphate minerals in terrestrial igneous and metamorphic rocks. In: Jerome Nriagu, J.O., Moore, P.B. (Eds.), Phosphate Minerals. Springer, Berlin, Heidelberg, pp. 215–241.

Olsen, E., Fuchs, L.H., 1967. The state of oxidation of some iron meteorites. Icarus 6, 242–253.

Omran, A., Abbatiello, J., Feng, T., Pasek, M.A., 2022. Oxidative phosphorus chemistry perturbed by minerals. Life (Basel) 12, 198.

Palme, H., Fegley, B., 1990. High-temperature condensation of iron-rich olivine in the solar nebula. Earth. Planet. Sci. Lett. 101, 180–195.

Pantaleone, S., Corno, M., Rimola, A., Balucani, N., Ugliengo, P., 2022. Water interaction with Fe_2NiP Schreibersite (110) surface: a quantum mechanical atomistic perspective. J. Phys. Chem. C 126, 2243–2252.

Pasek, M.A., 2017. Schreibersite on the early Earth: scenarios for prebiotic phosphorylation. Geosci. Front. 8, 329–335.

Pasek, M., 2019a. A role for phosphorus redox in emerging and modern biochemistry. Curr. Opin. Chem. Biol. 49, 53–58.

Pasek, M.A., 2019b. Phosphorus volatility in the early solar nebula. Icarus 317, 59–65.

Pasek, M.A., Dworkin, J.P., Lauretta, D.S., 2007. A radical pathway for organic phosphorylation during schreibersite corrosion with implications for the origin of life. Geochim. Cosmochim. Acta 71, 2243–2252.

Pasek, M.A., Kee, T.P., Bryant, D.E., Pavlov, A.A., Lunine, J.I., 2008. Production of potentially prebiotic condensed phosphates by phosphorus redox chemistry. Angew. Chem. Int. Ed. 47, 7918–7920.

Pasek, M.A., Gull, M., Herschy, B., 2017. Phosphorylation on the early earth. Chem. Geol. 475, 149–170.

Pasek, M.A., Lauretta, D.S., 2005. Aqueous corrosion of phosphide minerals from iron meteorites: a highly reactive source of prebiotic phosphorus on the surface of the early Earth. Astrobiology 5, 515–535.

Pasek, M., Lauretta, D., 2008. Extraterrestrial flux of potentially prebiotic C, N, and P to the early Earth. Orig. Life. Evol. Biosph. 38, 5–21.

Pasek, M.A., Omran, A., Feng, T., Gull, M., Lang, C., Abbatiello, J., Garong, L., Johnson, R., Ryan, J., Abbott-Lyon, H., 2022. Serpentinization as a route to liberating phosphorus on habitable worlds. Geochim. Cosmochim. Acta 336, 332–340.

Pirim, C., Pasek, M.A., Sokolov, D.A., Sidorov, A.N., Gann, R.D., Orlando, T.M., 2014. Investigation of schreibersite and intrinsic oxidation products from Sikhote-Alin, Seymchan, and Odessa meteorites and Fe3P and Fe2NiP synthetic surrogates. Geochim. Cosmochim. Acta 140, 259–274.

Rindlisbacher, M.A., Weisberg, M.K., Ebel, D.S., Alpert, S.P., 2021. Metal-rich nodules in anomalous EL3 chondrite Northwest Africa (NWA) 8785. Meteorit. Planet. Sci. 56, 960–970.

Rubin, A.E., 1997. Mineralogy of meteorite groups. Meteorit. Planet. Sci. 32, 231–247.

Rubin, A.E., Ma, C., 2017. Meteoritic minerals and their origins. Geochemistry 77, 325–385.

Rubin, A.E., Ma, C., 2021. Meteorite mineralogy, first ed. Cambridge University Press, Cambridge, United Kingdom.

Satterly, J., 1977. A catalogue of the Ontario localities represented by the mineral collection of the Royal Ontario Museum. Ont. Geol. Sun. Misc. Pap. 70.

Schaible, M.J., Pinto, H.P., McKee, A.D., Leszczynski, J., Orlando, T.M., 2019. Characterization and simulation of natural pyrite surfaces: a combined experimental and theoretical study. J. Phys. Chem. C 123, 26397–26405.

Smith, J.V., 1981. Halogen and phosphorus storage in the Earth. Nature 289, 762–765.

Sorensen-Stowell, K., Hengge, A.C., 2005. Examination of P− OR bridging bond orders in phosphate monoesters using ^{18}O isotope shifts in ^{31}P NMR. J. Org. Chem. 70, 4805–4809.

Turner, B.L., Mahieu, N., Condron, L.M., 2003. The phosphorus composition of temperate pasture soils determined by NaOH–EDTA extraction and solution ^{31}P NMR spectroscopy. Org. Geochem. 34, 1199–1210.

Walton, C.R., Baziotis, I., Cernok, A., Ferrière, L., Asimow, P.D., Shorttle, O., Anand, M., 2021. Microtextures in the Chelyabinsk impact breccia reveal the history of Phosphorus-Olivine-Assemblages in chondrites. Meteorit Planet Sci. 56, 742–766.

Wolf, D., Palme, H., 2001. The solar system abundances of phosphorus and titanium and the nebular volatility of phosphorus. Meteorit. Planet. Sci. 36, 559–571.

Zolensky, M.E., Nakamura, K., Gounelle, M., Mikouchi, T., Kasama, T., Tachikawa, O., Tonui, E., 2002. Mineralogy of Tagish Lake: an ungrouped type 2 carbonaceous chondrite. Meteorit. Planet. Sci. 37, 737–761.